Zonal Detached Eddy Simulation of the flow dynamics on an Ariane 5-type afterbody

P. E. Weiss⋆ *and S. Deck*⋆
⋆*ONERA, Applied Aerodynamics Department*
8, rue des Vertugadins, 92190 Meudon, France

Abstract

The present work focuses on the numerical simulation of a turbulent three-dimensional axisymmetric step. The objective of the paper is to assess the effect of the geometry on the dynamics of the separated flow. To this end, two geometries are considered. The first one is representative of the Ariane 5 main stage while the second one is an axisymmetric base with a smaller cylindrical extension tested at ONERA S3Ch continuous transonic wind tunnel and simulated by Weiss *et al.*[1] The results are compared with the available experimental data from the ONERA S3Ch campaigns. The spatial organization of the coherent structures is qualitatively shown. First and second order statistics exhibit pressure drops at the wall due to the abrupt changes of geometry in the nozzle region. One- and two- point spectral analysis evidenced the spatial limit of the predominant frequency. The differences between the two separating/reattaching flows are discussed in connection to the side loads whose characteristic frequencies are shifted.

1. Introduction

1.1 Context

The understanding of unsteady separating/reattaching flows as well as the related side loads has been significantly improved using validated hybrid RANS/LES simulations of ZDES-type (see Deck and Thorigny[2] and Weiss *et al.*[1]). However, the geometrical influence of the Ariane 5 afterbody on the dynamics of the massively separated flow is still poorly understood. Furthermore, the issue of the representativeness of a simplified configuration consisting in an axisymmetric backward facing step remains open. In particular, its effect on the spatial distribution of the azimuthal mode $m = 1$ related to the frequency $St_D = 0.2$, which is partially linked to the occurrence of side loads on the afterbodies, has not been clearly evidenced.

1.2 Organization of the paper

Following the previous introduction, a second part will be devoted to the description of the test cases and the numerical aspects involved in ZDES simulations. Then, results are divided into two parts. Firstly, the instantaneous flow field is investigated to distinguish the effects of the sudden changes of geometry respectively in terms of qualitative properties and Reynolds averaged data such as the streamwise evolution of mean and rms pressure coefficients. Secondly, the spatial organization of the fluctuating field is evidenced thanks to a one- and two-point spectral analysis. Finally, the differences are quantified in terms of rms load levels.

2. Numerical Set Up

2.1 Test Cases

The dimensions of the geometry of the Ariane 5 afterbody (scale $1 : 60$) and the simplified axisymmetric backward facing step were chosen to fit respectively with the experiments of the NLR (see Geurts[3]) and the experiments of the ONERA's S3Ch continuous research wind tunnel described by Deprés *et al.*[4] and later Meliga *et al.*[5] For both cases, the three-dimensional configuration is composed of an axisymmetric afterbody with a diameter D and an extension L resulting in a L/D ratio of 1.2 (see figure 1(a) for a sum up of the characteristic dimensions of the geometry, the mean flow topology and the main phenomena on the ONERA S3Ch configuration). The configuration is placed into a flow with a free stream Mach number of 0.7 for the ONERA S3Ch case and $M = 0.8$ for the axisymmetric Ariane 5 configuration implying a Reynolds number based on the forebody diameter, $Re_D \approx 1.2 \times 10^6$. Finally, the initial external boundary layer thickness δ was obtained modelling the necessary length for the forebody to have a δ/D ratio equal to 0.2 for the ONERA S3Ch case and $\delta/D = 0.1$ for the NLR configuration.

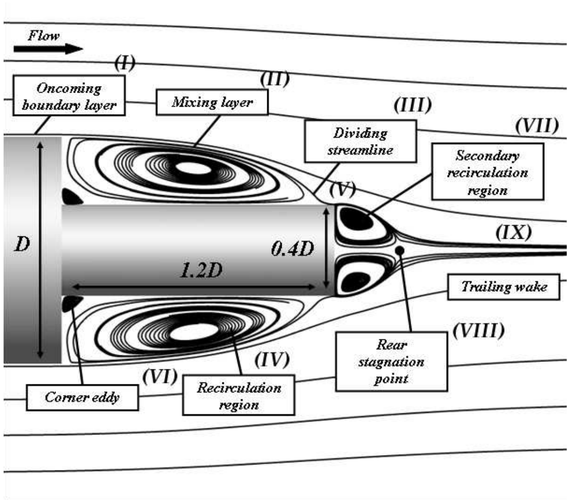

(a) Characteristic dimension and main topological phenomena of the simplified central afterbody

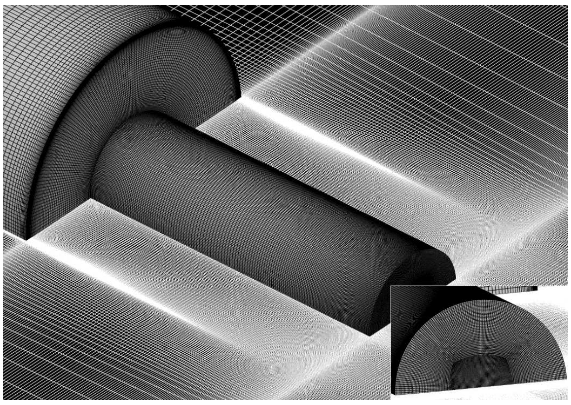

(b) Cutaway through the 3D mesh

Figure 1: Characteristics of the configuration derived from the ONERA S3Ch experiments

2.2 Grids

The definition of an adapted mesh for a hybrid RANS/LES simulation of ZDES-type is of primary importance. The mesh determines the ratio between the resolved and the modelled part of the turbulence. Table 1 summarizes the main characteristics of the 3D axisymmetric meshes. For the axisymmetric Ariane 5 case (called “A5 AXI” in the following), a surface visualization of the mesh is provided in figure 2(a). The mesh is structured and multiblock (see figure 2(b)) and contains 24.10^6 points. The azimuthal refinement is 1.5 degrees per plane i.e. 240 planes in the θ-direction. The configuration formerly designed from ONERA S3Ch experiments includes almost 12 millions hexaedric cells and has also 240 planes through the θ-direction. This configuration is named “S3Ch AXI” from now on.

For both configurations, the mesh has been built to fit with the LES requirements in the detached areas as regard the cell stretching and isotropy (see figure 1(b)). As advised by Simon *et al.*,[6] the early stages of the vorticity thickness development are modelled with a 15-point-resolution which then rapidly increases with the mixing layer growth up to almost a 60-point-resolution in the region of impingement of the mixing layer. Downstream the rear-body, an O-

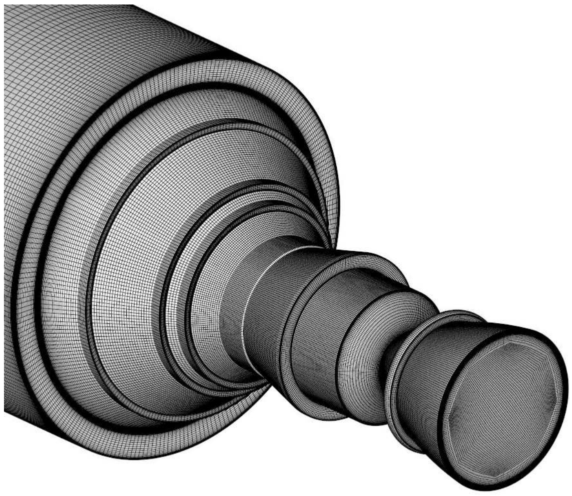

(a) Surface mesh

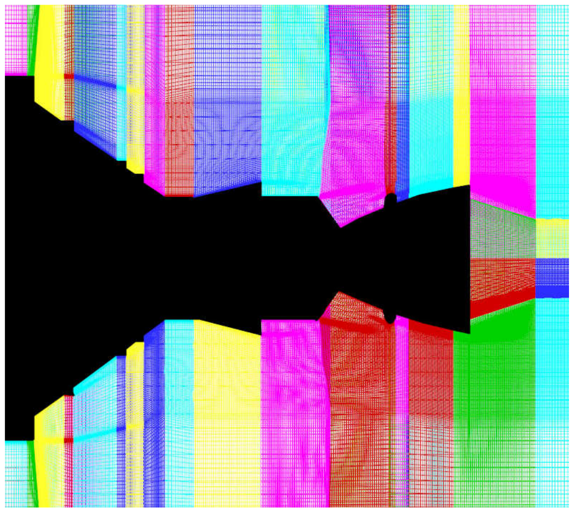

(b) Longitudinal view of the multiblock mesh

Figure 2: Views of the mesh of the central part of the axisymmetric Ariane 5 configuration without protuberances

H topology has been set to avoid singularity problem near the axis. Finally, the computations are performed on a NEC-SX8 over a total duration for the useful unsteady calculation of $T.U_\infty/H = 1580$. The timestep is equal to 2 μs providing acceptable Courant Friedrich-Levy (CFL) numbers (see table 1) based on the maximum acoustic velocity $(U + c)$.

Parameters	S3Ch AXI	A5 AXI
$N_x \times N_y \times N_z$	12.10^6	24.10^6
$N_z(\Delta\theta)$	240	240
N_x on the emergence (for $0 \leqslant x \leqslant L$)	171	256
N_y on the base (for $0.2 \leqslant y/D \leqslant 0.5$)	70	70
CFL_{max} in the mixing layer	around 7 excepted very locally at the separation edge 55	
CFL_{max} in the rest of the base flow	lower than 2	

Table 1: Grid characteristics

2.3 Zonal Detached Eddy Simulation (ZDES)

The approach used to model the flow is the Zonal Detached Eddy Simulation (ZDES) proposed by Deck[7,8] which belongs to the RANS/LES approaches (for more details see the discussion of Sagaut *et al.*[9]). ZDES has proved to be efficient to simulate complex turbulent phenomena in such high Reynolds number configurations (see Deck and Thorigny[2] or Simon *et al.*[6,10]). ZDES lets the user select RANS and DES areas. In our present case, the motivation related to the use of ZDES was to model the area downstream the separated point of the boundary layer, which is geometrically defined, with LES. Finally, the upstream part is computed using an URANS model, which ensures the incoming boundary layer to have the expected integral properties.

2.4 FLU3M Code

The finite-volume solver FLU3M for the compressible Navier-Stokes equations developed by ONERA was used to perform the simulations on multiblock structured grids. The approximation of time derivatives were carried out using the Gear scheme presented by Péchier *et al.*[11] which is backward in time and second-order accurate. The spatial scheme is a modified AUSM+(P) scheme, proposed by Mary and Sagaut.[12] The accuracy of the solver for DNS, LES, and hybrid RANS/LES purposes has been assessed in various applications including transitional flows around a two-dimensional wing profile in near-stall conditions,[12] after-body flows,[13] cavity flows at high Reynolds number,[14] and synthetic jets in a cross flow.[15] In these last references, the numerical results are thoroughly compared with the available experimental data including spectral and second-order analysis.

3. Results and Discussion

3.1 Instantaneous flowfield

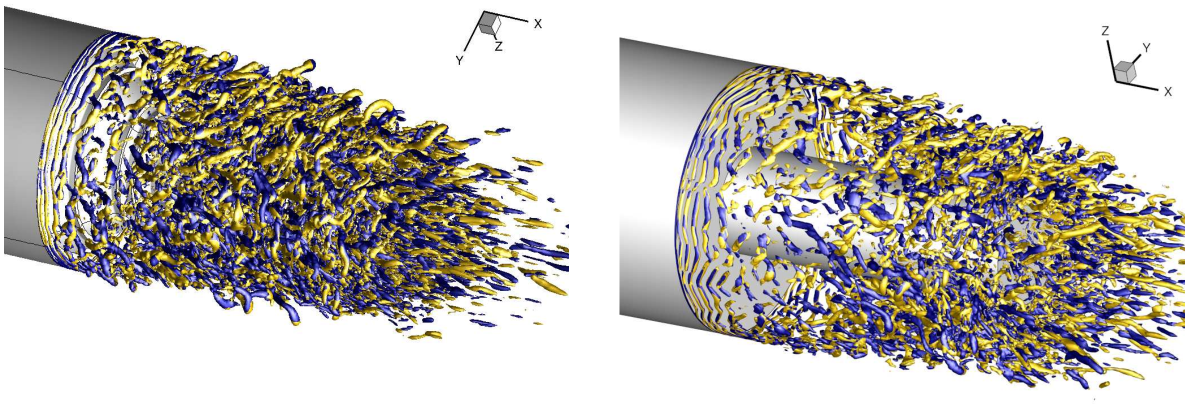

(a) A5 AXI

(b) S3Ch AXI

Figure 3: Visualization of the coherent structures downstream the two configurations with their related rotation (Isosurface of Q criterion such as $Q.U_\infty^2/D^2 = 100$ colored by the sign of the streamwise vorticity)

The detection of turbulent structures preserving a temporal coherence can constitute a first step to identify the main active zones of the flow dynamics. This qualitative overview of the spatial organization of the flow can be obtained through the analysis of the instantaneous flowfield.

The instantaneous behaviour of the flow is depicted for both cases (A5 AXI and S3Ch AXI) in figures 3(a) and 3(b). The turbulent structures are evidenced with a positive value of the second invariant of the velocity gradient tensor Q. In these figures, several characteristic structures of the separated afterbody flows can be distinguished. For both cases, a roll-up of toroidal eddies occurs with rapid pairings overwhelmed by large scale eddies which are highly three-dimensional. Theses structures develop until the mixing layer approaches the reattaching point. Moreover, hairpin-type structures appear near the reattachment. After the dislocation of the vortex pairing, the main structures are elongated along the streamwise direction of the flow.

In the A5 AXI case, the vortex pairing of the mixing layer arises earlier after the separation than for the S3Ch AXI configuration. This can be explained by the geometrical differences between the two cases. Indeed, the tronconic form of the base with its three small steps seems more destabilizing for the development of the A5 AXI shear layer than the abrupt base flow of the S3Ch AXI case. Furthermore, the amount of coherent structures produced in the second part of the emergence is higher. Such a difference can originate from this fast destabilization of the mixing process and from the geometrical changes existing on the nozzle.

3.2 Reynolds averaged data

The streamwise evolution of the wall pressure coefficient Cp for the cases A5 AXI and S3Ch AXI (see figure 4(a)) allows to distinguish the different steps of the recompression process in the recirculation zone located over the emergence. In both cases, for $x/D \leqslant 0$, a slow decrease is observed as the abscissa increase. This evolution emphasizes the influence of the mean pressure in the recirculation area on the base of larger cylinder, upstream from the separation.
Then, in a part of the separated region ranging from $x/D = 0$ to $x/D = 0.5$, the acceleration of the backflow leads to a diminution of the wall pressure coefficient. For $0 < x/D < 0.3$, the mixing process arises at a quasi-constant pressure. For the A5 AXI case, this process is locally slightly disturbed by the three consecutive changes in the geometry on the tronconic base. Beyond this zone, a strong recompression occurs in the confluence region where a maximum of the mean pressure coefficient $Cp_{max} \approx 0.1$ is reached just downstream the reattaching point for $x/D \approx 1.15$. The recompression process is globally of equal intensity as for the S3Ch AXI case. However, the increase of Cp is not

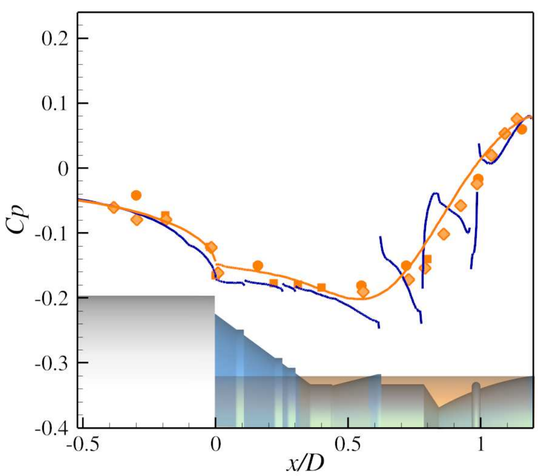

(a) Mean wall pressure coefficient Cp

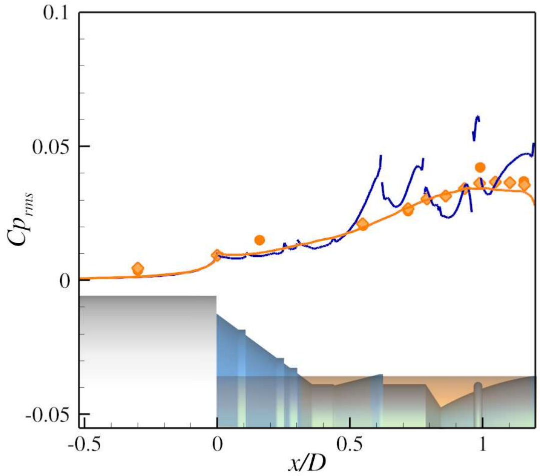

(b) RMS wall pressure coefficient Cp_{rms}

Figure 4: First and second order statistics of the wall pressure for the A5 AXI and S3Ch AXI test cases. ◆ : Meliga *et al.*[16] (kulites), ● : Deprés *et al.*[17] (kulites), ■ : Deprés *et al.*[17] (steady tabs), —— : ZDES of the ONERA S3Ch axisymmetric configuration, —— : ZDES of the axisymmetric Ariane 5 test case

monotonic. Indeed, for $x/D \in [0.6, 0.8]$ and $x/D \in [0.8, 0.95]$, the changes of section are sufficiently significant to induce local mixing and recompression processes. The presence of a toroidal shape on the nozzle near $x/D = 1$ gives a noticeable peak of Cp showing the potential occurrence of stronger turbulent phenomena.

The streamwise evolution of the *rms* pressure coefficient $Cp_{rms} = \overline{P'^2}/\frac{1}{2}\rho_\infty U_\infty^2$ is shown in figure 4(b)for the experimental and numerical configurations of Ariane 5 and S3Ch-type. The areas containing strong pressure fluctuations are evidenced in this figure. For the S3Ch AXI configuration, the fluctuation level increases monotonically until reaching a plateau just upstream from the mean reattachment location of the shear layer ($Cp_{rms} \approx 0.035$). This value confirms the one determined experimentally by Meliga *et al.*[16] at $x/D \approx 0.9$.

As for the Cp values, the growth of the wall pressure fluctuations in the A5 AXI case is not monotonic due to the sudden geometrical changes. Let us be reminded that Hudy *et al.*[18] have related this growth to the coherent structures of the shear layer which are intensifying impinging at the wall. The *rms* maxima noticed near the ring of the nozzle are twice as high as these of the S3Ch AXI case. Finally, the Cp_{rms} levels for the A5 AXI case are in a very good agreement with the full Ariane 5 configuration in the plane normal to the boosters.

3.3 One- and two- point spectral analysis

The power spectral densities show the frequency distribution of the fluctuating energy. To obtain a spatial representation of the spectral content, the power spectral density is computed over a total duration of 200 ms with a resolution equal to 60 Hz along a line of numerical pressure sensors at the wall. To enhance the location of the characteristic frequencies in space, an azimuthal average of the spectral maps obtained along the 240 generating lines of the emergence is realized (see figures 5(a) and 5(b)). For both separated flows, three zones can be distinguished. From $x/D = 0$ to $x/D = 0.2$, the energy is concentrated in the low frequency range between $St_D = 0$ and $St_D = 0.2$. At the opposite, near the nozzle ($0.8 < x/D < 1.2$), the highest energy levels related to the impinging structures of the shear layer are observed for higher frequencies ($St_D = 0.4$).

The main difference between the A5 AXI and S3Ch AXI configurations is noticed near the center of the emergence ($0.3 < x/D < 0.7$). Two zones of high energy with different streamwise extents are evidenced. For the S3Ch AXI case, the highest energy values are located in a zone ranging from $x/D = 0.4$ to $x/D = 0.7$ for a dimensionless frequency of 0.2. The A5 AXI configuration also has a localised area for this specific Strouhal number but over a more limited distance concentrated between $x/D = 0.45$ and $x/D = 0.55$ with a maximum reached at $x/D = 0.5$.
The spatial organization of the flow at these frequencies can also be considered through the analysis of the azimuthal

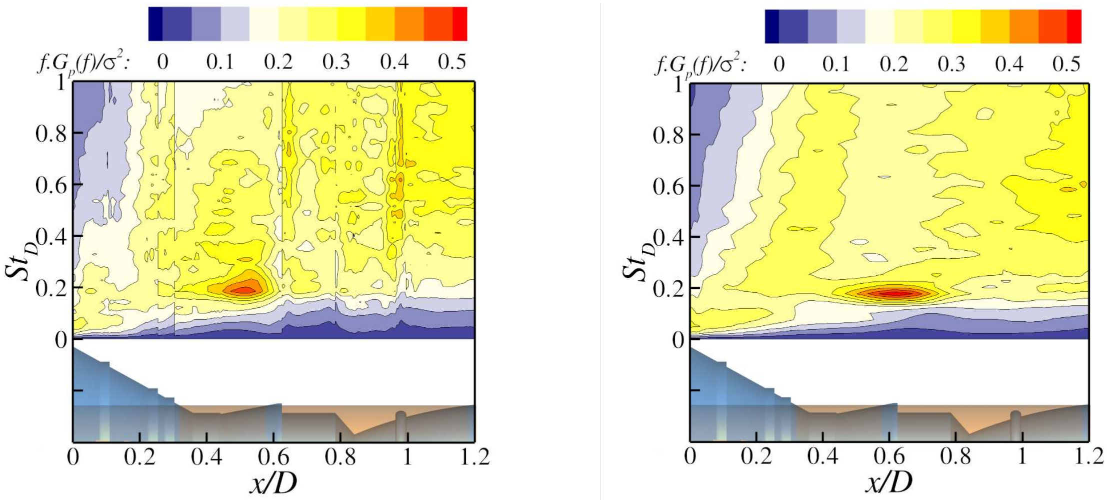

(a) A5 AXI

(b) S3Ch AXI

Figure 5: Azimuthal mean of the one-point spectral maps of the fluctuating wall pressure along the 240 generating lines of the emergence

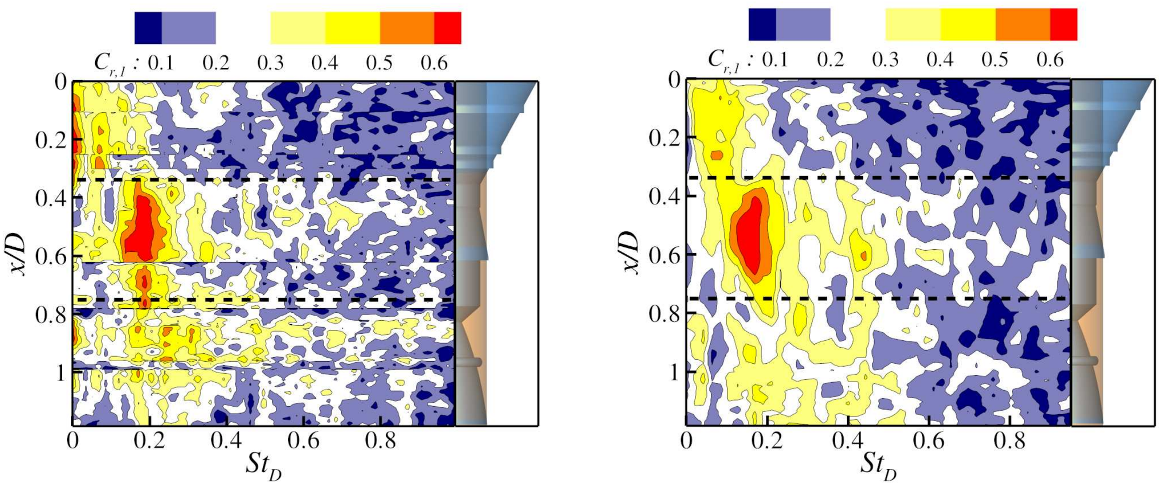

(a) A5 AXI - $m = 1$

(b) S3Ch AXI - $m = 1$

Figure 6: Spectral maps of the coherence function for the fluctuating wall pressure decomposed into azimuthal Fourier modes ($m = 0$ and $m = 1$). - - : limits of the absolute area for the $m = 1$ mode formerly determined by Weiss *et al.*[1] with a ZDES of the ONERA S3Ch test case

coherence of two pressure sensors $p_1(r, x, \phi_1)$ and $p_2(r, x, \phi_2)$ located in a plane normal to the inflow at a constant position x and a constant radius r. Assuming the hypothesis of an homogeneous flow, i.e. without any preferred angle of reference ϕ_1, the complex coherence function may be expressed as:

$$
\begin{aligned}
C(f, r, x, \Delta\phi) &= (C_r + jC_i)(f, r, x, \Delta\phi) \\
&= \frac{S_{12}(f, r, \Delta\phi, x)}{\sqrt{S_1(f, r, \phi_1, x)\, S_2(f, r, \phi_2, x)}}
\end{aligned}
\tag{1}
$$

where $j = \sqrt{-1}$, C_r and C_i are the real and imaginary parts of the cross-spectral density function S_{12} and $\Delta\phi = \phi_1 - \phi_2$, respectively. Assuming the disturbances do not exhibit any particular direction of propagation one has $S_{12}(\Delta\phi) = S_{12}(-\Delta\phi)$. Besides, the hypothesis of isotropy yields $C_i = 0$. Consequently, the C_r function is 2π periodic with respect to $\Delta\phi$ and can be expressed thanks to a Fourier transform in azimuthal modes:

$$
C_r(f, \Delta\phi) = \sum_{m=0}^{\infty} C_{r,m}(f) \cos(m\Delta\phi) \tag{2}
$$

$C_{r,m}$ represents the percentage of the fluctuating energy at frequency f relative to the azimuthal mode m since $\sum_m C_{r,m} = 1$. Let us be reminded that $m = 0$ and $m = 1$ modes are respectively characterized by an in-phase and anti-phase relationship of signals recorded simultaneously at two diametrically opposed locations. Then, a $C_{r,m}$ spectrum has been plotted for every streamwise location providing a spectral layer (figures 6(a) and 6(b)). These figures exhibit the highest percentages of the fluctuating energy for Strouhal numbers St_D based on the forebody diameter close to 0.2 which are localized between $x/D \approx 0.35$ and $x/D \approx 0.75$ for the S3Ch AXI case and between $x/D \approx 0.35$ and $x/D \approx 0.60$ for the A5 AXI case.

Thus, the relation between the characteristic frequency $St_D = 0.2$ and the antisymmetric azimuthal mode $m = 1$, already identified for the S3Ch AXI case by Weiss *et al.*,[1] is also found here for the A5 AXI case. As a consequence, the ONERA S3Ch test case seems to well reproduce the main features of the flow for the real afterbody geometry without any protuberances and boosters. However, the influence of the sudden changes of geometry on the flow of the A5 AXI case is not negligible and is well apparent on the spatial extent of the characteristic frequency.

3.4 Dynamic buffet loads

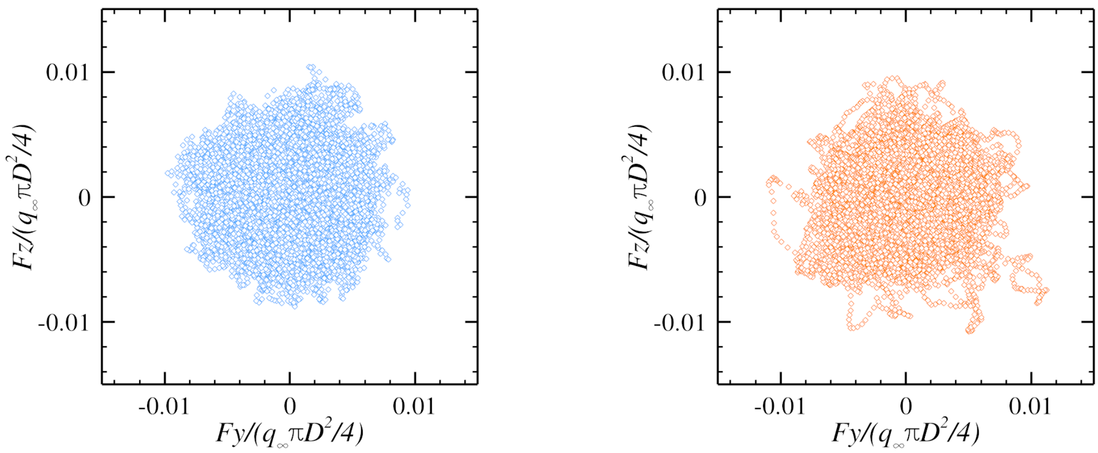

(a) A5 AXI - $m = 1$

(b) S3Ch AXI - $m = 1$

Figure 7: Polar plots of the dimensionless buffet loads along z ($Fz/(q_\infty \pi D^2/4)$) as a function of the loads along y ($Fy/(q_\infty \pi D^2/4)$). ◇ : ZDES of the Ariane 5 axisymmetric test case, ◇ : ZDES of the ONERA S3Ch axisymmetric configuration

The polar plots represented in figures 7(a) and 7(b) show the evolution of the side forces for the two calculations A5 AXI and S3Ch AXI. These figures exhibit the dimensionless value of the load $C_{Fz}(t) = Fz(t)/(q_\infty \pi D^2/4)$ as a function of $C_{Fy}(t) = Fy(t)/(q_\infty \pi D^2/4)$. The side loads have similar values for both cases. Moreover, the highly coherent fluctuations at the wall induce the asymmetric unsteady loads. These loads can be obtained integrating the unsteady pressure field at the wall of the emergence during the calculation. One can notice the isotropic (i.e. $\sigma_{Fy} = \sigma_{Fz}$) and random character of the fluctuating loads. The envelop of the efforts is circular and centered around zero since a temporally-averaged axisymmetric flow produces no load (i.e. $\overline{Fy} = \overline{Fz} = 0$).

The spectrum of the side loads allows to compare more precisely the efforts on both configurations. Figure 8 represents the energy of the side loads for the A5 AXI and S3Ch AXI cases as a function of the dimensionless frequencies. The axisymmetric cases show very similar distributions of the fluctuating energy for the side loads integrated along the emergence. The distribution of the fluctuating energy is broadband and, in the zone of the proeminent peak, the frequency range between $St_D = 0.1$ and $St_D = 0.3$ contributes to almost 60% of the energy of the side loads. Furthermore, the broadband character of the spectrum for the axisymmetric afterbody reveals the presence of a complex turbulent process responsible for the growth of the instabilities.

Regarding the values of the Strouhal number, the occurrence of strong peaks has been mentionned for the two cases. However, the magnitude of these peaks and the dimensionless frequency for the afterbody of "axisymmetric Ariane

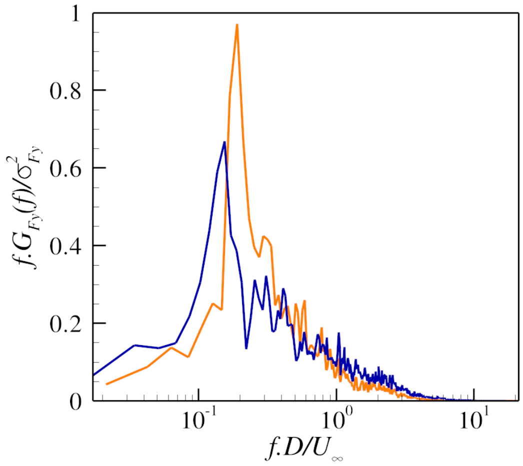

Figure 8: Normalized spectrum of the y-component of the load as a function of the Strouhal number St_D based on the diameter of the upstream cylinder. ▬ : ZDES of the ONERA S3Ch axisymmetric configuration, ▬ : ZDES of the Ariane 5 axisymmetric test case

5"- and S3Ch-type differ. Indeed, the strong peak of the A5 AXI configuration for a Strouhal number equal to 0.19 is approximatively 1.5 times lower in terms of magnitude than for the S3Ch AXI case centered around $St_D = 0.15$.

Table 2 gathers the mean and rms side load values denoting the axisymmetry of the flow. Then, the rms levels of the side loads reflect a similar production of buffet loads.

	$\overline{C_{Fy}}$	$\overline{C_{Fz}}$	$\overline{C'^2_{Fy}}$	$\overline{C'^2_{Fz}}$
S3Ch AXI	$-2,76.10^{-5}$	$-4,66.10^{-4}$	$2,89.10^{-3}$	$2,84.10^{-3}$
A5 AXI	$5,02.10^{-5}$	$7,08.10^{-4}$	$2,80.10^{-3}$	$2,76.10^{-3}$

Table 2: Mean and standard deviation of the normal components of the computed effort for the simulations of the ONERA S3Ch case and the Ariane 5 configuration without any protuberances and boosters

4. Conclusion

The objective of the present paper was to improve the physical understanding of the dynamics of a massively separated flow for a real and an academic axisymmetric configuration.

The influence of the geometry of the central part of the Ariane 5 afterbody without protuberances on the dynamics of the flow has been compared for the experimental and numerical results available for the ONERA S3Ch configuration with an L/D ratio equal to 1.2 and a Mach number equal to 0.7. A ZDES simulation has been prepared and performed taking advantage of the methodology used for the former simulation realized on a more academic case (ONERA S3Ch). Comparing the statistical values of wall pressure of this new simulation with the data of the S3Ch AXI case tested experimentally in the ONERA S3Ch transonic wind tunnel, it appears that the ZDES simulation fits the distribution and the levels measured.

The different changes of geometry of the A5 AXI configuration has shown to disturb the development of the mixing layer leading to a higher production of small-scale turbulent structures. The Cp_{rms} maximum, due to the presence of a ring on the nozzle, becomes almost twice as high going from 3% of the dynamic pressure for the S3Ch AXI configuration to almost 6% for the A5 AXI case. However, the global topology has appeared close to the S3Ch AXI one. Moreover, the dynamics of the flow has shown to be led by a dimensionless frequency near $St_D = 0.2$ and related to the antisymmetric azimuthal mode $m = 1$. However, the massive one- and two-point spectral analysis have pointed out that this frequency as well as its associated mode are localised in a more limited area.

To sum up, the dynamics of the A5 AXI case has shown to be well represented by the S3Ch AXI case regarding the main features of the flow. Moreover, the formerly used methodology remains efficient to calculate such type of afterbody flows. Finally, the abrupt changes of geometry and the ring in the nozzle region are the elements responsible for the alteration of the spatial organization of the fluctuating field compared to an academic case.

Acknowledgments

The authors thank the Centre National d'Etudes Spatiales (CNES) for financial support within the framework of the research and technology program ATAC (aerodynamics of nozzles and after-bodies).

References

[1] Weiss, P., Deck, S., Robinet, J.-C., and Sagaut, P., "On the dynamics of axisymmetric turbulent separating/reattaching flows," *Physics of Fluids*, Vol. 21, 2009, pp. 075103.

[2] Deck, S. and Thorigny, P., "Unsteadiness of an axisymmetric separating-reattaching flow," *Physics of Fluids*, Vol. 19, No. 065103, 2007.

[3] Geurts, E., "Steady and unsteady pressure measurements on the rear section of various configurations of the Ariane 5 launch vehicle," *6th International Symposium on Launcher Technologies, Munich, Germany, November*, 2005.

[4] Deprés, D., Reijasse, P., and Dussauge, J. P., "Analysis of Unsteadiness in Afterbody Transonic Flows," *AIAA Journal*, Vol. 42, No. 12, December 2004, pp. 2541–2550.

[5] Meliga, P. and Reijasse, P., "Unsteady Transonic Flow behind an Axisymmetric Afterbody with Two Boosters," *Proceedings of the 25th AIAA Applied Aerodynamics Conference*, Miami, 2007, pp. 1–8.

[6] Simon, F., Deck, S., Guillen, P., Sagaut, P., and Merlen, A., "Numerical simulation of the compressible mixing layer past an axisymmetric trailing edge," *Journal of Fluid Mechanics*, Vol. 591, 2007, pp. 215–253.

[7] Deck, S., "Zonal-detached-eddy simulation of the flow around a high-lift configuration," *AIAA Journal*, Vol. 43, No. 11, November 2005, pp. 2372–2384.

[8] Deck, S., "Numerical simulation of transonic buffet over a supercritical airfoil," *AIAA Journal*, Vol. 43, No. 7, July 2005, pp. 1556–1566.

[9] Sagaut, P., Deck, S., and Terracol, M., *Multiscale and multiresolution approaches in turbulence*, Imperial College Press, 2006.

[10] Simon, F., Deck, S., Guillen, P., and Sagaut, P., "Reynolds Averaged Navier Stokes / Large Eddy Simulations of supersonic base flow," *AIAA Journal*, Vol. 44, No. 11, 2006, pp. 2578 – 2590.

[11] Péchier, M., Guillen, P., and Caysac, R., "Magnus Effect over Finned Projectiles," *AIAA Journal of Spacecraft and Rockets*, Vol. 38, No. 4, 2001, pp. 542–549.

[12] Mary, I. and Sagaut, P., "Large eddy simulation of flow around an airfoil near stall," *AIAA Journal*, Vol. 40, No. 6, 2002, pp. 1139–1145.

[13] Deck, S., Garnier, E., and Guillen, P., "Turbulence Modelling Applied to Space Launcher Configurations," *Journal of Turbulence*, Vol. 3, No. 1, 2002.

[14] Larchevêque, L., Labbé, O., Mary, I., and Sagaut, P., "Turbulence Modelling Applied to Space Launcher Configurations," *Physics of Fluids*, Vol. 15, No. 193, 2003.

[15] Dandois, J., Garnier, E., and Sagaut, P., "Numerical Simulation of Active Separation Control by a Synthetic Jet," *Journal of Fluid Mechanics*, Vol. 574, 2007, pp. 25–58.

[16] Meliga, P. and Reijasse, P., "Unsteady transonic flow behind an axisymmetric afterbody with two boosters," *Proceedings of the 25th AIAA Applied Aerodynamics Conference, No. 2007-4564, Miami, June*, 2007.

[17] Deprés, D., Reijasse, P., and Dussauge, J. P., "Analysis of unsteadiness in afterbody transonic flows," *AIAA Journal*, Vol. 42, No. 12, December 2004, pp. 2541–2550.

[18] Hudy, L. M., Naguib, A. M., and Humphreys, W. M., "Wall-pressure-array measurements beneath a separating/reattaching flow region," *Physics of Fluids*, Vol. 15, No. 706, 2003.